RESEARCH ARTICLE

Staphylococcus aureus Fibronectin-Binding Protein A Mediates Cell-Cell Adhesion through Low-Affinity Homophilic Bonds

Philippe Herman-Bausier,[a] Sofiane El-Kirat-Chatel,[a] Timothy J. Foster,[b] Joan A. Geoghegan,[b] Yves F. Dufrêne[a]

Université catholique de Louvain, Institute of Life Sciences, Louvain-la-Neuve, Belgium[a]; Department of Microbiology, Trinity College Dublin, Dublin, Ireland[b]

P.H.-B. and S.E.-K.-C. contributed equally to this article.

ABSTRACT ***Staphylococcus aureus* is an important opportunistic pathogen which is a leading cause of biofilm-associated infections on indwelling medical devices. The cell surface-located fibronectin-binding protein A (FnBPA) plays an important role in the accumulation phase of biofilm formation by methicillin-resistant *S. aureus* (MRSA), but the underlying molecular interactions are not yet established. Here, we use single-cell and single-molecule atomic force microscopy to unravel the mechanism by which FnBPA mediates intercellular adhesion. We show that FnBPA is responsible for specific cell-cell interactions that involve the FnBPA A domain and cause microscale cell aggregation. We demonstrate that the strength of FnBPA-mediated adhesion originates from multiple low-affinity homophilic interactions between FnBPA A domains on neighboring cells. Low-affinity binding by means of FnBPA may be important for biofilm dynamics. These results provide a molecular basis for the ability of FnBPA to promote cell accumulation during *S. aureus* biofilm formation. We speculate that homophilic interactions may represent a generic strategy among staphylococcal cell surface proteins for guiding intercellular adhesion. As biofilm formation by MRSA strains depends on proteins rather than polysaccharides, our approach offers exciting prospects for the design of drugs or vaccines to inhibit protein-dependent intercellular interactions in MRSA biofilms.**

IMPORTANCE ***Staphylococcus aureus* is a human pathogen that forms biofilms on indwelling medical devices, such as central venous catheters and prosthetic joints. This leads to biofilm infections that are difficult to treat with antibiotics because many cells within the biofilm matrix are dormant. The fibronectin-binding proteins (FnBPs) FnBPA and FnBPB promote biofilm formation by clinically relevant methicillin-resistant *S. aureus* (MRSA) strains, but the molecular mechanisms involved remain poorly understood. We used atomic force microscopy techniques to demonstrate that FnBPA mediates cell-cell adhesion via multiple, low-affinity homophilic bonds between FnBPA A domains on adjacent cells. Therefore, FnBP-mediated homophilic interactions represent an interesting target to prevent MRSA biofilms. We propose that such homophilic mechanisms may be widespread among staphylococcal cell surface proteins, providing a means to guide intercellular adhesion and biofilm accumulation.**

Received 11 March 2015 **Accepted** 16 April 2015 **Published** 26 May 2015

Citation Herman-Bausier P, El-Kirat-Chatel S, Foster TJ, Geoghegan JA, Dufrêne YF. 2015. *Staphylococcus aureus* fibronectin-binding protein A mediates cell-cell adhesion through low-affinity homophilic bonds. mBio 6(3):e00413-15. doi:10.1128/mBio.00413-15.

Invited Editor Victor J. Torres, New York University School of Medicine **Editor** Gerald B. Pier, Harvard Medical School

Address correspondence to Joan A. Geoghegan, geoghegj@tcd.ie, or Yves F. Dufrêne, Yves.Dufrene@uclouvain.be.

Staphylococcus aureus is a human commensal and opportunistic pathogen that causes both superficial and invasive infections (1, 2). This species is a major cause of infections associated with indwelling medical devices such as central venous catheters and prosthetic joints (1, 2). The ability to form biofilms on implanted devices results in infections that are difficult to treat with antibiotics because many cells within the biofilm matrix are dormant. This is compounded by the prevalence of strains that are resistant to multiple antibiotics (methicillin-resistant *S. aureus* [MRSA]) (3, 4). Consequently, understanding the molecular mechanisms leading to the formation of staphylococcal biofilms may contribute to the development of novel therapeutic approaches for combating biofilm-related infections.

Until recently, the accumulation phase of *S. aureus* biofilms was attributed solely to the elaboration of polysaccharide intercellular adhesin (PIA), also known as poly-*N*-acetylglucosamine (PNAG) (1, 2, 5). However, it is now clear that proteins that are covalently anchored to the cell wall by sortase (cell wall-anchored proteins) can also promote biofilm accumulation. In the cases of SraP, SdrC, and SasG, cell-cell interactions have been shown to be due to specific homophilic binding between protein molecules located on adjacent cells (2, 5).

The fibronectin (Fn)-binding proteins (FnBPs) FnBPA and FnBPB promote biofilm formation by clinically relevant MRSA strains, both community associated and hospital associated (6–8). Both FnBPA and FnBPB have N-terminal A domains that are structurally and functionally related to clumping factor A (ClfA) and the *Staphylococcus epidermidis* SdrG protein and bind to fibrinogen by a variation of the dock, lock, and latch (DLL) mechanism whereby conformational changes in subdomains N2 and N3 within the A region result in highly stabilized complexes (9–11). The C-terminal fibronectin-binding domain comprises tan-

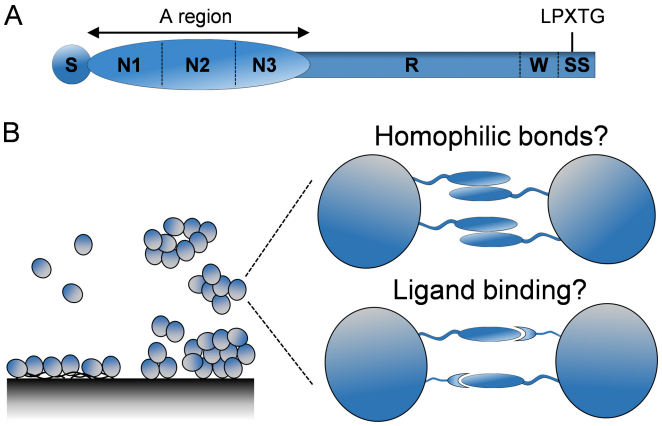

FIG 1 FnBPA-dependent biofilm formation. (A) Schematic representation of the *S. aureus* FnBPA protein: S, secretory signal sequence; the A region comprising N1, N2, and N3 subdomains involved in fibrinogen and elastin binding and cell-cell aggregation during biofilm formation; R, tandem repeats of fibronectin-binding domains; W, proline-rich cell wall-spanning region; SS, sorting signal comprising the LPXTG motif, membrane-spanning domain, and positively charged tail. (B) Role of FnBPA in biofilm formation. In a first stage, FnBPA proteins promote attachment to host plasma proteins on biomaterial surfaces (left part of the left cartoon). Then, FnBPA mediates cell aggregation and biofilm accumulation (right part of the left cartoon). Whether this is achieved by homophilic protein-protein interactions or by binding to other ligands on adjacent cells is not yet established (right cartoons).

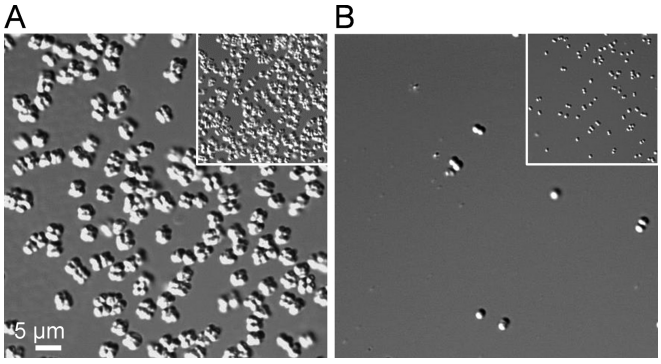

FIG 2 FnBPA-mediated adhesion to fibronectin. Optical (differential interference contrast) images showing the microscopic adhesion behavior of FnBPA$^+$ cells (A) and FnBPA$^-$ cells (B), after a 2-h incubation on Fn-coated surfaces. Insets are representative images from a duplicate experiment.

dem repeats that are intrinsically disordered, resulting in an extended flexible "stalk" that projects the A domain from the cell surface (Fig. 1A). The biofilm-forming region of FnBPA was localized to subdomains N2 and N3 of the N-terminal A region, but accumulation was shown not to involve a DLL mechanism (6, 7). FnBP-promoted biofilms could involve direct homophilic interactions or binding of the proteins to surface-located receptors on adjacent cells (Fig. 1B) (2).

Atomic force microscopy (AFM) has provided valuable insights into the molecular basis of staphylococcal adhesion. Force spectroscopy with biospecific probes has been used to probe the localization and binding strength of adhesins, including FnBPs, down to the single-molecule level (12–16). Furthermore, the use of bacterial cell probes has enabled the quantification of cell-substrate and cell-cell adhesive forces at the whole-cell level (17–19). In this study, we explore the molecular mechanism of FnBPA-dependent cell-cell adhesion using these AFM techniques (20, 21). Specifically, we address the following questions: how strong are intercellular bonds, how many FnBPA proteins do they involve, and is FnBPA-mediated intercellular adhesion achieved by means of homophilic interactions or ligand binding? We analyze the binding mechanism of full-length FnBPA expressed from a plasmid in *S. aureus* strain SH1000 defective in clumping factors (Clfs) A and B, and in FnBPA and FnBPB (here *S. aureus* FnBPA$^+$ cells), as well as of the recombinant FnBPA A domain immobilized on model surfaces. The results demonstrate that FnBPA mediates specific cell-cell adhesion via multiple, low-affinity homophilic bonds that depend on Zn^{2+} ions and involve the A domain.

RESULTS

FnBPA is involved in fibronectin binding and in cell aggregation. We first confirmed that FnBPA adhesins were expressed on FnBPA$^+$ bacteria by analyzing their ability to adhere to Fn-coated substrates at the microscopic scale. Optical microscopy showed that FnBPA$^+$ cells adhered strongly to Fn-coated surfaces, unlike FnBPA$^-$ cells, which hardly adhered at all (Fig. 2). Consistent with published data, this shows that FnBPA promotes bacterial adhesion to Fn and that the adhesin is expressed appropriately on FnBPA$^+$ cells described here.

We then studied the involvement of FnBPA in cell-cell adhesion (Fig. 3). Figure 3A to C shows that FnBPA$^+$ cells resuspended in buffer were isolated, without any evidence for aggregation. Addition of 1 mM Zn^{2+} induced the formation of large aggregates, 5 μm to 5 mm in size (Fig. 3D to F). Cell aggregates were disrupted in the presence of 1 mM EDTA (Fig. 3G to I) but restored upon further addition of Zn^{2+} (Fig. 3J to L). Aggregation was much less pronounced in *S. aureus* cells expressing no FnBPA (FnBPA$^-$ cells; Fig. 3M to O). These results show that FnBPA mediates cell-cell adhesion via Zn^{2+}-dependent interactions.

Force spectroscopy of FnBPA interactions. AFM-based force spectroscopy was applied to living bacteria and to purified proteins to investigate the forces driving FnBPA-mediated cell-cell adhesion (Fig. 4). We used single-cell force spectroscopy (SCFS) (22, 23) to quantify the adhesion forces between single *S. aureus* cells. Single FnBPA$^+$ cells were attached on colloidal cantilevers coated with polydopamine, allowing us to record force-distance curves between the cellular probes and the edges of small cell aggregates adhering on solid substrates (Fig. 4A). Single-molecule force spectroscopy (SMFS) was employed to probe single FnBPA bonds on live cells (Fig. 4B). Recent work showed that the region required for biofilm formation by FnBPA localizes to residues 166 to 498 of the A domain (7). Recombinant full-length FnBPA A domain was covalently bound to AFM tips in a random orientation, and the modified tips were used to record force-distance curves on FnBPA$^+$ cells immobilized in porous membranes. To probe single FnBPA-FnBPA bonds in the absence of any other interactions, forces were also measured between tips and substrates both functionalized with fully oriented recombinant A domains (Fig. 4C).

FnBPA promotes specific cell-cell adhesion forces. We measured the adhesion forces between two individual *S. aureus* cells. Adhesion forces, rupture lengths, and typical force signatures obtained for three representative pairs of FnBPA$^+$ cells are shown in Fig. 5A and B (see also Fig. S1 in the supplemental material for data obtained on more cells). Many curves featured large adhesion

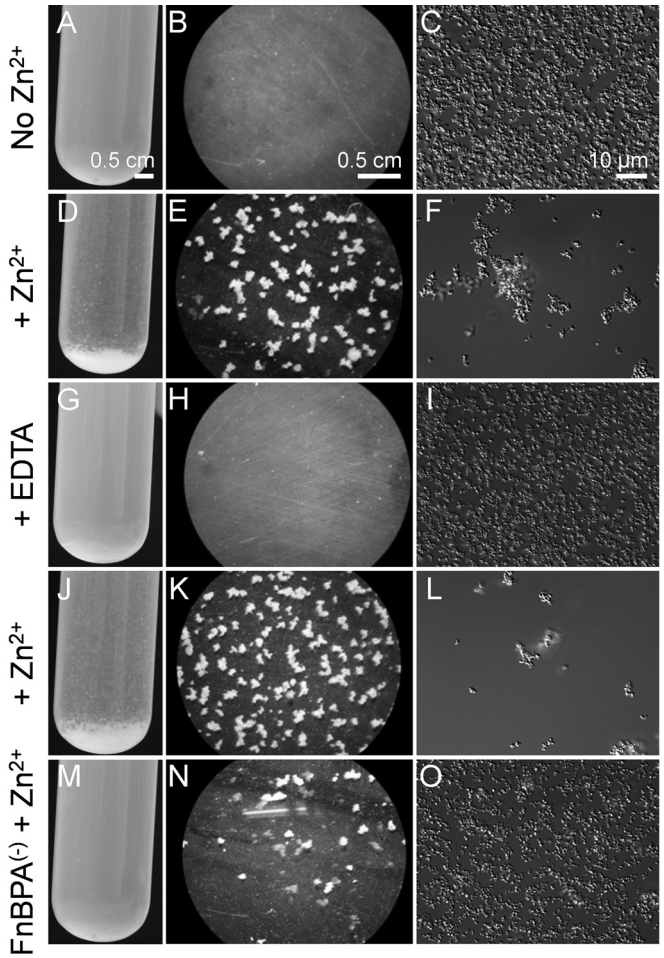

FIG 3 Role of FnBPA in cell aggregation. (A to L) Stereomicrographs (A, D, G, and J) and low- (B, E, H, and K) and high-resolution (C, F, I, and L) optical microscopy images of *S. aureus* cells expressing FnBPA (FnBPA$^+$ cells) after resuspension in TBS buffer (A to C), resuspension in TBS buffer containing 1 mM Zn^{2+} (D to F), addition of 1 mM EDTA (G to I), and further addition of 1 mM Zn^{2+} (J to L). (M to O) Control experiment using an *S. aureus* strain expressing no FnBPA (FnBPA$^-$ cells), in TBS with 1 mM Zn^{2+}.

force peaks of 250- to 3,000-pN magnitude and 150- to 500-nm rupture length (cell 1, 1,966 ± 470 pN, 351 ± 83 nm, mean ± standard deviation [SD] on $n = 98$ adhesive curves; cell 2, 834 ± 424 pN, 294 ± 68 nm, $n = 470$; cell 3, 1,640 ± 514 pN, 327 ± 73 nm, $n = 223$). There were some variations from one cell pair to another (see also Fig. S1), which may reflect cellular heterogeneity as well as small variations in cell-cell contact area. Discrete rupture steps were often seen before rupture of the main adhesion peak, suggesting that multiple bonds were involved. However, adhesion peaks generally showed sharp ruptures, implying that, upon stretching, the different bonds detached simultaneously.

Do cell adhesion forces involve FnBPA proteins? We found that EDTA dramatically decreased the adhesion probability (Fig. 5C and D; also see Fig. S2 in the supplemental material), consistent with the notion that FnBPA interactions require Zn^{2+} ions (7). As can be seen in Fig. 5E and F (see also Fig. S2), we also measured the forces between *S. aureus* FnBPA$^-$ cells that lack FnBPA. Most adhesion events were abolished, indicating that the large adhesion forces on FnBPA$^+$ cells involve FnBPA proteins. Intriguingly, the same effect was observed for the interaction between FnBPA$^+$ and FnBPA$^-$ cells (Fig. 5G and H; see also Fig. S2). This suggests that interaction between two FnBPA$^+$ cells involves FnBPA proteins located on the two cell surfaces. So, our single-cell experiments show that FnBPA proteins on the *S. aureus* cell surface mediate specific, zinc-dependent, cell-cell interactions.

Binding strength of single FnBPA proteins on living bacteria. How strong is a single FnBPA bond? To address this question, we analyzed the forces between recombinant FnBPA A domains attached to AFM tips and full-length FnBPA proteins on FnBPA$^+$ cells (Fig. 6; see also Fig. S3 in the supplemental material). Figure 6A to C (see Fig. S3 for more cells) shows that a large fraction (~50%) of the force curves recorded across three different cells featured single adhesion peaks with a moderate force of 125 ± 65 pN (mean ± SD from a total of 3,072 curves obtained on three cells). We believe that these forces originate from single FnBPA bonds as (i) adhesion was strongly decreased upon addition of EDTA (Fig. 6D to F; see also Fig. S3), when using *S. aureus* FnBPA$^-$ cells (Fig. 6G to I; see also Fig. S3), or when using bare tips (see Fig. S3); (ii) the A domains were attached at low density on the tip; and (iii) the measured forces are in the range of the binding force typically reported for single-cell adhesion proteins (24, 25). Presumably, the larger adhesion forces sometimes detected (200 to 300 pN) are due to multiple FnBPA bonds. How does the measured bond strength compare with that reported for Fn-FnBP bonds? Our ~125-pN force is stronger than the ~60-pN force measured for single Fn-FnBP bonds at a similar loading rate (12, 15), suggesting that different mechanisms are involved. Strikingly, several groups have reported much larger adhesion forces for Fn-FnBP interactions, up to 6 nN depending on the strain investigated (13, 14, 16). However, the authors attached Fn at high density on the tip, meaning that many Fn-FnBP bonds were probed in parallel (up to 80). This is an important difference from the present work, in which FnBPA A domains were covalently attached at low density on the tip to favor single-bond detection.

Adhesion force maps indicate that the adhesins were largely exposed on the cell surface. Assuming that each adhesion event in the maps represents the detection of a single FnBPA, we find that the protein is exposed at a surface density of ~2,000 proteins/μm^2. In earlier work, the distribution of adhesins was mapped on the surface of staphylococcal cells. Immunogold electron microscopy was used to study the distribution of SssF and UafB adhesins on *Staphylococcus saprophyticus* (26, 27). While the authors claimed that there was abundant labeling, the density was lower than that here, an effect that may reflect actual differences between species or variations in the sensitivity of the techniques. AFM force mapping was also used to map FnBPs on staphylococcal cells (15, 28). Lower et al. (15) revealed the spatial localization of putative FnBPs on *S. aureus* bacteria deposited on different substrates. Results suggested that the production and localization of FnBP proteins may be induced by an external stimulus, such as the presence of Fn on a surface.

Do the observed rupture lengths, 98 ± 44 nm (mean ± SD; 3 different cells), compare with the lengths of the probed molecules? As the full-length FnBPA protein and its His-tagged A domain are 948 and 481 amino acids in length (6, 7), respectively, and assuming that each amino acid contributes 0.36 nm to the contour length of a fully extended polypeptide chain (29), the lengths of fully extended proteins and A domains are expected to be 341 nm and 173 nm, respectively. Full extension of the A domain-FnBPA

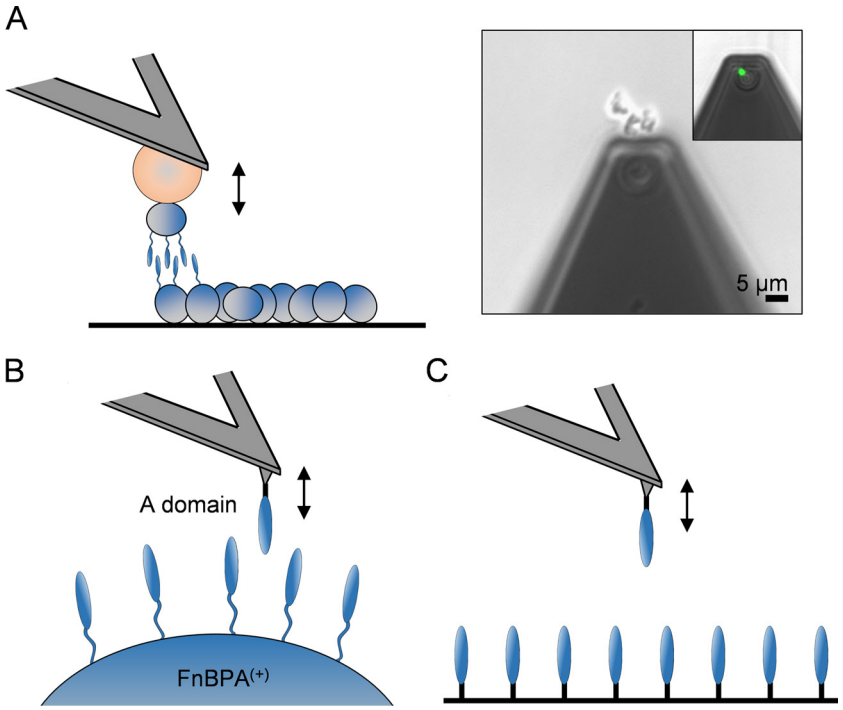

FIG 4 Force spectroscopy of FnBPA interactions. (A) To investigate cell-cell adhesion forces with SCFS, living bacteria were attached on polydopamine-coated colloidal cantilevers and force curves were obtained between cellular probes and small bacterial aggregates. The right micrograph shows a cell probe cantilever approaching a cell aggregate. The inset is a fluorescence image of a single bacterium attached to the colloidal probe. (B) To analyze single FnBPA bonds on living bacteria with SMFS, bacterial cell surfaces were probed using AFM tips labeled with the recombinant A domain. (C) To study single FnBPA homophilic bonds by SMFS, force curves were recorded between AFM tips and substrates functionalized with the recombinant A domain.

complex should therefore lead to a length of about 500 nm, which is much longer than what we observed. This means that the bond ruptures before complete unfolding of the proteins and, hence, that the latter are mechanically stable. This observation agrees well with earlier single-molecule results showing that SdrG, which shares strong structural similarities with FnBP, is not completely unfolded when subjected to large forces (30). We note that longer extensions were observed for cell-cell bonds (Fig. 5), supporting the notion that they involve pairs of full-length FnBPA proteins.

How many FnBPA bonds are involved in a cell-cell bond? As a rough estimate, this number may be inferred by comparing our single-molecule (Fig. 6) and single-cell (Fig. 5) forces and by considering the interaction area between two cells. The contact zone of two deformable spheres pressed on each other may be described by the Hertz model (31): $A = (3FR/4E^{*})^{1/3}$, in which A is the radius of the contact area, R is the effective radius ($1/R = 2/r$, where r is the cell radius), F is the applied load (here, 250 pN), and E^{*} is the effective Young modulus [$1/E^{*} = (2 - 2\nu^{2})/E$, in which E is the elastic moduli and ν is the Poisson ratio associated with the cell]. Assuming that the *S. aureus* cell radius r is 0.5 μm, the Young modulus is 1.8 MPa (32), and the Poisson ratio is 0.3, we found an area radius of ~36 nm, thus yielding a contact area of ~0.004 μm^2. What is the number of interacting molecules in this area? Considering a surface density of ~2,000 FnBPA proteins/μm^2, as determined above from the force maps, the adhesion forces measured between two cells would involve about 8 FnBPA proteins in parallel on each cell. Given the variability of the data and the assumptions made in the model, this is in the range of the value obtained by comparing the adhesion forces measured for single molecules and single cells (~125 versus 800 to 2,000 pN). This leads us to believe that FnBPA-dependent cell-cell adhesion involves about 10 cumulative bonds, as also indicated by the sharp peak ruptures.

FnBPA mediates low-affinity homophilic bonds. To explain how FnBPA mediates cell-cell adhesion, two possible mechanisms were recently postulated, i.e., homophilic interactions or receptor-ligand binding (7) (Fig. 1B). Although our single-cell results are in favor of homophilic bonds, a direct demonstration for these was still lacking. We therefore measured the forces and dynamics of the interaction between purified FnBPA A domains in the absence of any other cell wall components (Fig. 4C). Force measurements between A domains revealed adhesion events with a mean adhesion force of 182 ± 78 pN (Fig. 7A, inset), which we attribute to single FnBPA-FnBPA bonds as A domains were uniformly oriented at low density on the two interacting surfaces. The measured strength is slightly larger than that between the A domain and full-length FnBPA on cells, an effect that could reflect differences in the orientation and accessibility of the molecules. The ~180-pN force is much weaker than the 2-nN force measured for SdrG-Fg bonds (30), indicating that FnBPA-mediated cell-cell adhesion does not involve a DLL binding mechanism. FnBPA-FnBPA bonds showed extensions (~50 nm) that were much shorter than those on live cells, suggesting that the A domains were hardly unfolded.

We then explored the dynamics of the FnBPA-FnBPA interaction, with the aim to assess the affinity of the bond. The forces needed to rupture homophilic bonds have been shown to depend on the loading rate, i.e., the rate at which the force is applied to the complex (24, 25, 33, 34). In agreement with this, we found that the

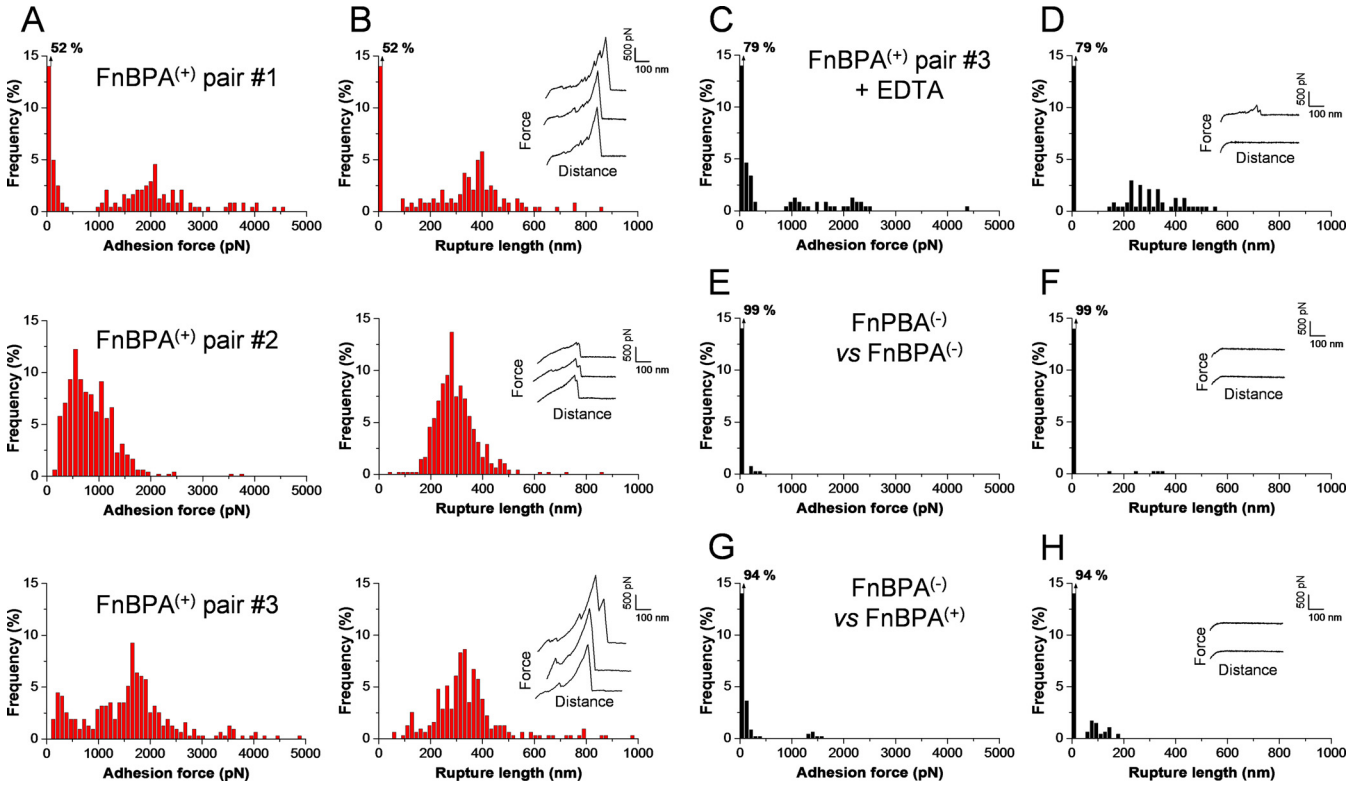

FIG 5 Cell-cell force spectroscopy of FnBPA bonds. (A and B) Adhesion force histograms (A) and rupture length histograms (B) with representative force signatures (insets), obtained by recording multiple force-distance curves in TBS supplemented with 1 mM Zn^{2+} between three pairs of interacting $FnBPA^{+}$ cells. (C and D) Force data obtained under the same conditions (cell 3) following addition of 1 mM EDTA. (E to H) Force data obtained under the same conditions for the interaction between two *S. aureus* $FnBPA^{-}$ cells (E and F) and between $FnBPA^{+}$ and $FnBPA^{-}$ cells (G and H). All curves were obtained using a contact time of 1 s, a maximum applied force of 250 pN, and approach and retraction speeds of 1,000 nm · s^{-1}.

mean adhesion force (F) between two A domains increases linearly with the logarithm of the loading rate (r), as illustrated in Fig. 7A. The length scale of the energy barrier, x_β, was assessed from the slope f_β of the F versus ln(r) plot and found to be 0.2 nm, i.e., in the range of values (0.2 to 1 nm) typically measured by single-molecule AFM. Extrapolation to zero forces yielded the kinetic off-rate constant of dissociation at zero force: $k_{off} = r_{F=0}\, x_\beta/k_B T = 0.11\ s^{-1}$. This high dissociation rate, similar to that of homophilic bonds in cadherins (33) and in bacterial trimeric autotransporter adhesins (24), suggests that FnBPA homophilic bonds are highly dynamic. This short duration of adhesion may contribute to biofilm dissemination, by helping the bacteria to rapidly detach and colonize new sites.

We also studied how the adhesion frequency (i.e., number of curves with adhesion events) varies with interaction time, while keeping the loading rate constant (Fig. 7B). The binding frequency increased to reach a plateau corresponding to almost 100% binding probability after only 0.5 s, indicating that bond formation is fast. Similar fast bond formation was also observed with cadherins (33). Considering the interaction time needed for half-maximal probability of binding, $t_{0.5} = 168$ ms, we assessed the association rate constant, $k_{on} = {t_{0.5}}^{-1} N_A V_{eff} = 7.5\ M^{-1}\ s^{-1}$, where V_{eff} is the effective volume explored by the tip-tethered protein (approximated here to a half-sphere of 1-nm radius) (35). We then estimated the equilibrium dissociation constant: $K_D = k_{off}/k_{on} = 15$ mM. The obtained K_D value is much higher than that for FnBPA binding to fibrinogen (~1 μM) (11) but in the range of that of homophilic interactions by trimeric autotransporter adhesins (24), thus indicating that homophilic FnBPA bonds have low affinity. This finding may have important biological implications. Low-affinity binding by means of FnBPA may represent the primary step in biofilm accumulation, enabling dynamic cell behaviors to occur, while subsequent higher-affinity binding would lead to firm cell-cell adhesion. In particular, the positively charged PIA polysaccharide, also known as poly-*N*-acetylglucosamine (PNAG), may enhance intercellular interactions by high-affinity multivalent binding with the negatively charged cell surfaces.

DISCUSSION

There is now considerable evidence that FnBPs participate in biofilm accumulation by *S. aureus* (6–8, 36), but the underlying molecular mechanisms are poorly understood. This study demonstrates that FnBPA mediates strong cell-cell adhesion via multiple, low-affinity homophilic bonds between A domains on adjacent cells. We speculate that homophilic interactions may be widespread among staphylococcal cell surface proteins, providing a means to promote intercellular adhesion and biofilm accumulation. Our methodology offers exciting prospects for the design of drugs or vaccines to inhibit protein-dependent intercellular interactions in MRSA biofilms.

The N2 and N3 subdomains of SdrC (37) have also been shown to promote cell-cell interactions, suggesting that homophilic interactions by these domains could be a general mechanism to promote the accumulation phase in *S. aureus* biofilms. Although the

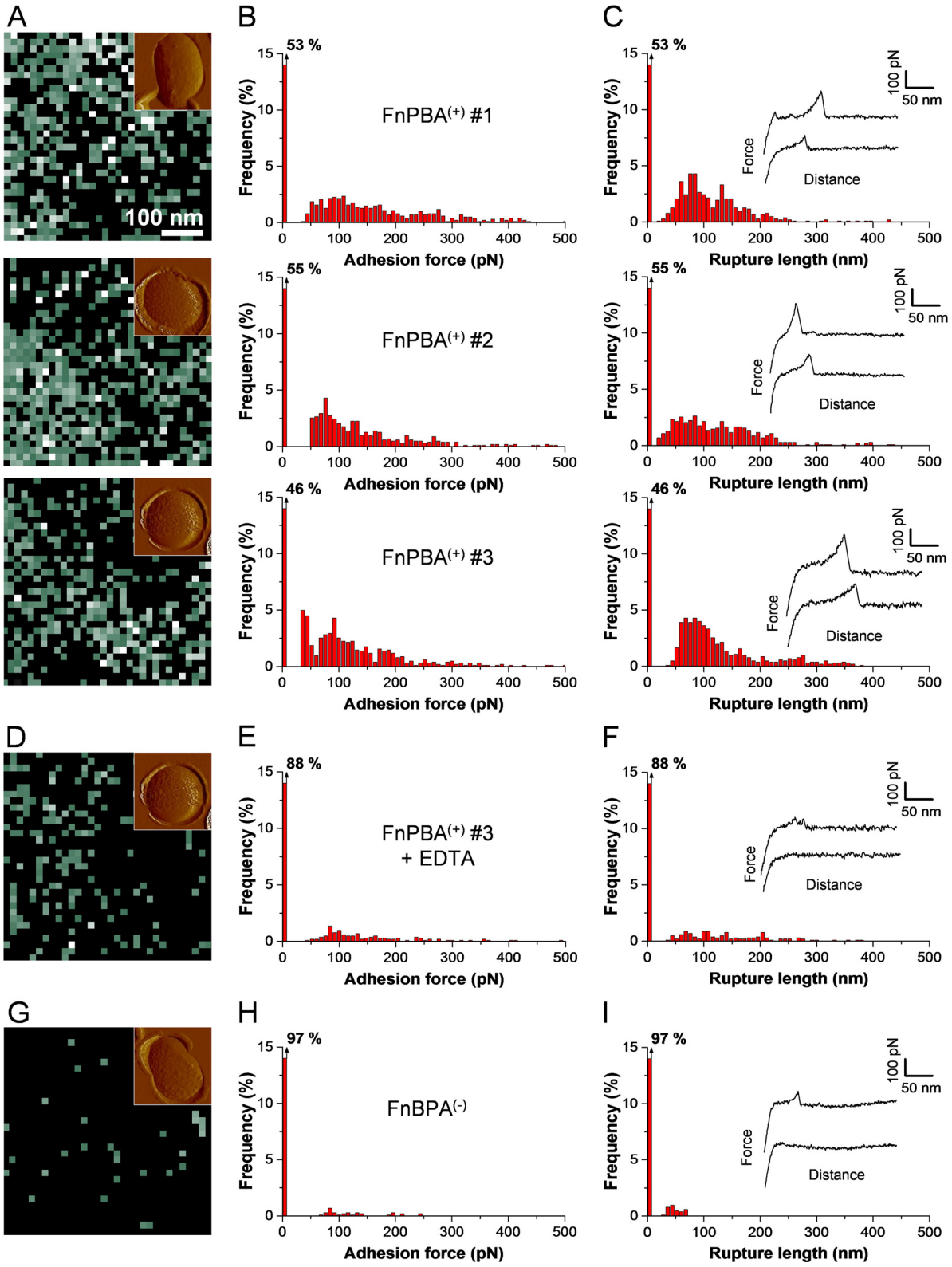

FIG 6 Single-molecule force spectroscopy of FnBPA bonds on living bacteria. (A to C) Adhesion force maps (500 nm by 500 nm; gray scale, 500 pN) (A), adhesion force histograms (B), and rupture length histograms (C) together with representative force curves obtained by recording force curves in TBS with 1 mM Zn^{2+} across the surface of three *S. aureus* FnBPA$^+$ cells using tips labeled with the FnBPA A domain. Shown in the insets in panel A are deflection images of the cells. (D to I) Force data obtained for an FnBPA$^+$ cell (cell 3) in the presence of 1 mM EDTA (D to F) and for an *S. aureus* FnBPA$^-$ cell (G to I). All curves were obtained using a contact time of 100 ms, a maximum applied force of 250 pN, and approach and retraction speeds of 1,000 nm · s^{-1}.

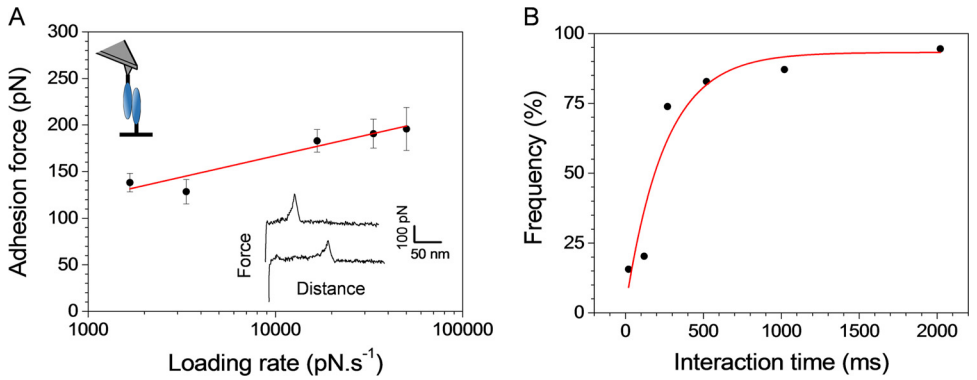

FIG 7 Force and dynamics of FnBPA homophilic interactions. (A) Dependence of the adhesion force on the loading rate applied during retraction, measured in TBS with 1 mM Zn^{2+} between a tip and a substrate both functionalized with FnBPA A domains, using a contact time of 100 ms and an approach speed of 1,000 nm · s^{-1} (mean ± standard error of the mean). The mean adhesion force (F) increased linearly with the logarithm of the loading rate (r): $F = 5.3 \times 10^{-11} \ln(r) + 2.0 \times 10^{-11}$. The R^2 value obtained for the linear fit was 0.85. Shown in the lower inset are representative force curves. (B) Dependence of the adhesion frequency on the interaction time, measured at a constant approach and retraction speed of 1,000 nm · s^{-1}. Similar loading rate and interaction time plots were obtained in multiple experiments using different tips and substrates.

structural details of FnBPA homophilic interactions are unclear, we speculate that they occur between residues on the surface of the N2 or N3 subdomains. In the case of SdrC, 2 amino acid sequences located within the N2 subdomain were found to act cooperatively to promote SdrC dimerization and, as a result, intercellular interactions (37). Whether a similar mechanism applies to FnBPA remains to be determined.

The occurrence of FnBPA homophilic bonds correlated with the cell aggregation behavior, leading us to believe that these interactions represent an important driving force for biofilm formation. Unlike the very strong and stable DLL bonds, homophilic bonds show moderate strength and fast dissociation, a trait which may be important for biofilm dissemination. Several factors can lead to biofilm detachment, including mechanical stress like fluid flow, and detachment agents like enzymes or surfactants (1, 38). Together with these factors, the fast dissociation of the FnBPA bonds may contribute to cell detachment (isolated cells or cell clusters), therefore favoring colonization of new sites.

Our finding that zinc is required to form homophilic bonds is consistent with earlier reports showing that FnBPA (7) but also other staphylococcal adhesins, like SasG (39) and Aap (40, 41), promote zinc-dependent biofilm accumulation. It is therefore tempting to speculate that *S. aureus* has evolved these subdomains to promote homophilic cellular interactions, thus providing a general mechanism to favor biofilm accumulation. The biological significance of the Zn^{2+}-dependent cell-cell interactions promoted by FnBPA can be called into question if the cation is limiting *in vivo*. The mammalian host restricts access to cations such as Zn and Mn that bacteria need for growth and proliferation *in vivo*, a phenomenon called nutritional immunity (42). An important host factor that contributes to this phenomenon is calprotectin, a Zn^{2+}-binding protein that can reach high levels in infected tissue (43). However, successful pathogens such as *S. aureus* produce dedicated uptake machinery for cations (42). It should be noted that Zn^{2+} is present in the cytosol of mammalian cells and bacteria (44). *S. aureus* lyses host cells by secreting cytolytic toxins which release cytoplasmic contents. In addition, during biofilm development, some of the bacterial cells undergo autolysis to release DNA, which is an important component of the biofilm matrix (45). This altruistic action will also release bacterial cytoplasmic contents, including Zn^{2+}. More than 3% of *Escherichia coli* proteins contain Zn^{2+} (46). The extracellular zinc-dependent metalloprotease aureolysin of *S. aureus* contributes to virulence in mice, indicating that it is active *in vivo* and presumably acquires its Zn^{2+} cofactor following secretion (47). We thus argue that the local concentration of Zn^{2+} at the early stages of biofilm development will be sufficient to support FnBP-mediated aggregation. Finally, the expression of FnBPs has been shown to support biofilm formation on subcutaneous catheters during experimental infections of mice, arguing that adequate Zn^{2+} is likely to be present *in vivo* (36).

MATERIALS AND METHODS

Bacterial strains and growth conditions. The *S. aureus* FnBPA$^-$ strain (strain SH1000 *clfA clfB fnbA fnbB*) is defective in clumping factors A and B and fibronectin-binding proteins A and B (6). FnBPA$^-$ cells were grown overnight in tryptic soy broth (TSB), washed once with TSB, subcultured into TSB at a 1:100 dilution, and allowed to grow to an optical density at 600 nm (OD_{600}) of 0.4. The *S. aureus* FnBPA$^+$ strain is a derivative of strain SH1000 *clfA clfB fnbA fnbB* carrying plasmid pFNBA4 expressing fibronectin-binding protein A from strain 8325-4 (7). For expression of FnBPA, FnBPA$^+$ cells were grown overnight in TSB with chloramphenicol (10 μg/ml), washed once in TSB, subcultured into TSB at a 1:100 dilution, and allowed to grow to an OD_{600} of 0.4 in TSB plus chloramphenicol.

Recombinant proteins. Plasmid pQE30::$FnBPA_{37–511}$ (10) was used as the template for inverse PCR with the phosphorylated primers 5′-TCA GAACAAAAGACAACTACAG-3′ and 5′-GGATCCCGATCCTCTCATA GTTAATTTCTC-3′ to eliminate DNA encoding the N-terminal His tag. The PCR product was treated with DpnI to eliminate template DNA, and following blunt-end ligation, the plasmid was transformed into *E. coli* XL1-Blue. The plasmid was extracted from *E. coli* and used as template for inverse PCR with phosphorylated primers 5′-CATCACCATCACCATCA CTAAGTCGACCTGCAGCCAAG-3’ and 5’-TTAATTTTTCTCATTTC CGTTCG-3’ to introduce an in-frame fusion with DNA encoding a C-terminal 6xHis tag. This PCR product was treated with DpnI, blunt-end ligation was carried out, and the plasmid was transformed into *E. coli* XL1-Blue. The C-terminally hexahistidine-tagged FnBPA A domain protein (residues 37 to 511) was expressed and purified by Ni^{2+} affinity chromatography as previously described (39).

Adhesion assay. To assess the adhesion phenotype of the bacterial strains, bacteria were incubated with Fn-coated substrates prepared as follows. Glass coverslips coated with a thin layer of gold were immersed

overnight in an ethanol solution containing 1 mM 10% 16-mercaptododecahexanoic acid–90% 1-mercapto-1-undecanol (Sigma), rinsed with ethanol, and dried with N_2. Substrates were then immersed for 30 min in a solution containing 10 mg · ml^{-1} *N*-hydroxysuccinimide (NHS) and 25 mg · ml^{-1} 1-ethyl-3-(3-dimethylaminopropyl)-carbodiimide (EDC) (Sigma), rinsed 5 times with Ultrapure water (ELGA LabWater), incubated with 0.1 mg · ml^{-1} of Fn from bovine plasma (Sigma) for 1 h, and rinsed further with phosphate-buffered saline (PBS) buffer. Fn substrates were incubated at 37°C in 200-μl bacterial suspensions adjusted in Tris-buffered saline (TBS) buffer supplemented with 1 mM $ZnCl_2$ to an OD_{600} of 0.3 to 0.4. After 2 h, the substrates were gently rinsed by 3 consecutive washes in TBS buffer supplemented with 1 mM $ZnCl_2$ and directly imaged using an inverted optical microscope (Zeiss Axio Observer Z1) equipped with a Hamamatsu C10600 camera.

Aggregation assays. Aggregation phenotypes were directly observed after cell resuspension in TBS buffer (pH 7.4) or TBS buffer supplemented with 1 mM $ZnCl_2$, addition of 1 mM EDTA, and further addition of 1 mM $ZnCl_2$. Aggregation levels were observed in test tubes, by optical microscopy at low magnification (Zeiss Stemi DV4 stereomicroscope; Oberkochen, Germany) and at high magnification (Zeiss Axio Observer Z1 equipped with a Hamamatsu C10600 camera; Oberkochen, Germany).

Cell-cell force spectroscopy. To probe bacterial aggregates with single-cell probes, hydrophobic substrates were prepared by coating glass coverslips with a thin layer of gold, immersing them overnight in a solution of 1 mM 1-dodecanethiol (Sigma-Aldrich), rinsing them with ethanol, and drying them under N_2. Cells resuspended in TBS buffer plus 1 mM $ZnCl_2$ were deposited and allowed to adhere on hydrophobic substrates for 2 h. Nonadhering cells were removed by gentle rinsing, and the cell-coated substrates were attached, while avoiding dewetting, to the bottom of a glass petri dish. Bacterial cell probes were obtained as previously described (22, 23). Briefly, colloidal probes were prepared by attaching a single silica microsphere (6.1-μm diameter; Bangs Laboratories) with a thin layer of UV-curable glue (NOA 63; Norland Edmund Optics) on triangular tipless cantilevers (NP-O10; Microlevers, Veeco Metrology Group) and using a Nanoscope VIII Multimode AFM (Bruker Corporation, Santa Barbara, CA). Cantilevers were then immersed for 1 h in 10 mM Tris buffer plus 150 mM NaCl solution (pH 8.5) containing 4 mg/ml dopamine hydrochloride (99%; Sigma), rinsed in Tris buffer plus 150 mM NaCl solution (pH 8.5), and used directly for cell probe preparation. The nominal spring constant of the colloidal probe cantilever was ~0.06 N/m as determined by the thermal noise method (Picoforce; Bruker). For cell probe preparation, 50 μl of a concentrated cell suspension was transferred into the glass petri dish containing the cell-coated hydrophobic substrates, after which 4 ml of TBS plus 1 mM $ZnCl_2$ was added to the system. The colloidal probe was brought into contact with an isolated bacterium, using a Bioscope Catalyst AFM (Bruker Corporation, Santa Barbara, CA) equipped with a Zeiss Axio Observer Z1 and a Hamamatsu C10600 camera. Optical microscopy was used to check for proper attachment of the cell, and the cell probe was positioned over the edge of a cell aggregate lying on the hydrophobic substrates. Cell probes were used to measure cell-cell interaction forces at room temperature (20°C), by recording multiple force curves, using a maximum applied force of 250 pN, a 1-s contact time, and constant approach and retraction speeds of 1,000 nm · s^{-1}. Adhesion force and rupture length histograms were obtained by calculating the maximum adhesion force and the last rupture distance for each curve. In total, 24 different cell probes were used to measure cell adhesion forces under standard and control conditions.

Single-molecule force spectroscopy on live cells. For SMFS on live cells, gold-coated AFM cantilevers with a nominal spring constant of ~0.02 N m^{-1} (OMCL-TR4; Olympus Ltd., Tokyo, Japan) were functionalized with FnBPA A domains at low density and with a random orientation (48). Cleaned gold cantilevers were immersed overnight in a 1 mM solution of 10% $HS(CH_2)_{16}COOH$ (Sigma-Aldrich) and 90% $HS(CH_2)_{11}OH$ (Sigma-Aldrich), rinsed with ethanol, immersed for 30 min in a solution containing 10 mg · ml^{-1} *N*-hydroxysuccinimide (NHS) (Sigma-Aldrich) and 25 mg · ml^{-1} 1-ethyl-3-(3-dimethylaminopropyl)-carbodiimide (EDC) (Sigma-Aldrich), and rinsed with water. The activated cantilevers were then incubated with 0.2 mg · ml^{-1} of recombinant FnBPA A domains in PBS for 2 h, followed by rinsing and storage in PBS. All probes were freshly prepared and used the same day. The spring constants of the cantilevers were measured using the thermal noise method (Picoforce; Bruker).

SMFS measurements were performed at room temperature (20°C) in TBS buffer plus 1 mM $ZnCl_2$ using a Nanoscope VIII Multimode AFM (Bruker Corporation, Santa Barbara, CA). Bacterial cells were immobilized by mechanical trapping into porous polycarbonate membranes (Millipore, Billerica, MA) with a pore size similar to the cell size. After filtering a cell suspension, the filter was gently rinsed with TBS plus 1 mM $ZnCl_2$, carefully cut (1 cm by 1 cm), and attached to a steel sample puck using a small piece of double-face adhesive tape, and the mounted sample was transferred into the AFM liquid cell while avoiding dewetting. First, bare probes were used to localize and image individual cells and then were replaced by A domain probes. Adhesion force maps were obtained by recording 32-by-32 force-distance curves on areas of 500 by 500 nm, calculating the adhesion force for each force curve, and displaying the adhesive events as gray pixels. All force curves were recorded at 100-ms contact time, with a maximum applied force of 250 pN, and using a constant approach and retraction speed of 1,000 nm/s.

Single-molecule force spectroscopy on model surfaces. SMFS measurements using tips and substrates functionalized with FnBPA A domains were performed at room temperature (20°C) in TBS buffer plus 1 mM $ZnCl_2$ using a Nanoscope VIII Multimode AFM (Bruker Corporation, Santa Barbara, CA). Recombinant FnBPA A domain with a C-terminal His tag was immobilized onto cantilevers and substrates as follows. Silicon substrates were coated by thermal evaporation with a thin layer of Cr (5 nm) followed by a thin layer of gold (30 nm). Gold substrates and gold cantilevers (see above) were rinsed in ethanol, cleaned for 10 min by UV-ozone treatment, rinsed in ethanol, and dried with N_2. They were immersed overnight in a 0.1 mM solution of 99% HS-C_{11}-$(EG)_3$-OH thiols (ProChimia) and 1% HS-C_{11}-$(EG)_3$-NTA thiols (ProChimia), rinsed with ethanol, dried with N_2, and immersed in a 40 mM aqueous solution of $NiSO_4$ (pH 7.2) for 30 min. Cantilevers and substrates were then incubated in a 200-μl droplet of a 200-μg/ml solution of FnBPA A domains for 1 h and rinsed and stored in PBS. Unless stated otherwise, multiple force curves were recorded at 100-ms contact time, with a maximum applied force of 250 pN, and using a constant approach and retraction speed of 1,000 nm/s.

SUPPLEMENTAL MATERIAL

Supplemental material for this article may be found at http://mbio.asm.org/lookup/suppl/doi:10.1128/mBio.00413-15/-/DCSupplemental.

Figure S1, PDF file, 1.3 MB.
Figure S2, PDF file, 1.3 MB.
Figure S3, PDF file, 1.6 MB.

ACKNOWLEDGMENTS

Work at the Université catholique de Louvain was supported by the National Fund for Scientific Research (FNRS); the Université catholique de Louvain (Fonds Spéciaux de Recherche); the Région Wallonne; the Federal Office for Scientific, Technical and Cultural Affairs (Interuniversity Poles of Attraction Programme); and the Research Department of the Communauté française de Belgique (Concerted Research Action). Y.F.D. is a Research Director of the FNRS.

REFERENCES

1. **Otto M.** 2008. Staphylococcal biofilms. Curr Top Microbiol Immunol **322:**207–228. http://dx.doi.org/10.1007/978-3-540-75418-3_10.
2. **Foster TJ, Geoghegan JA, Ganesh VK, Höök M.** 2014. Adhesion, invasion and evasion: the many functions of the surface proteins of *Staphylococcus aureus*. Nat Rev Microbiol **12:**49–62. http://dx.doi.org/10.1038/nrmicro3161.

3. **Chambers HF, Deleo FR**. 2009. Waves of resistance: *Staphylococcus aureus* in the antibiotic era. Nat Rev Microbiol **7:**629–641. http://dx.doi.org/10.1038/nrmicro2200.
4. **DeLeo FR, Otto M, Kreiswirth BN, Chambers HF**. 2010. Community-associated meticillin-resistant *Staphylococcus aureus*. Lancet **375:**1557–1568. http://dx.doi.org/10.1016/S0140-6736(09)61999-1.
5. **Speziale P, Pietrocola G, Foster TJ, Geoghegan JA**. 2014. Protein-based biofilm matrices in staphylococci. Front Cell Infect Microbiol **4:**171. http://dx.doi.org/10.3389/fcimb.2014.00171.
6. **O'Neill E, Pozzi C, Houston P, Humphreys H, Robinson DA, Loughman A, Foster TJ, O'Gara JP**. 2008. A novel *Staphylococcus aureus* biofilm phenotype mediated by the fibronectin-binding proteins, FnBPA and FnBPB. J Bacteriol **190:**3835–3850. http://dx.doi.org/10.1128/JB.00167-08.
7. **Geoghegan JA, Monk IR, O'Gara JP, Foster TJ**. 2013. Subdomains N2N3 of fibronectin binding protein A mediate *Staphylococcus aureus* biofilm formation and adherence to fibrinogen using distinct mechanisms. J Bacteriol **195:**2675–2683. http://dx.doi.org/10.1128/JB.02128-12.
8. **McCourt J, O'Halloran DP, McCarthy H, O'Gara JP, Geoghegan JA**. 2014. Fibronectin-binding proteins are required for biofilm formation by community-associated methicillin-resistant *Staphylococcus aureus* strain lac. FEMS Microbiol Lett **353:**157–164. http://dx.doi.org/10.1111/1574-6968.12424.
9. **Ponnuraj K, Bowden MG, Davis S, Gurusiddappa S, Moore D, Choe D, Xu Y, Hook M, Narayana SV**. 2003. A "dock, lock, and latch" structural model for a staphylococcal adhesin binding to fibrinogen. Cell **115:**217–228. http://dx.doi.org/10.1016/S0092-8674(03)00809-2.
10. **Keane FM, Loughman A, Valtulina V, Brennan M, Speziale P, Foster TJ**. 2007. Fibrinogen and elastin bind to the same region within the A domain of fibronectin binding protein A, an MSCRAMM of *Staphylococcus aureus*. Mol Microbiol **63:**711–723. http://dx.doi.org/10.1111/j.1365-2958.2006.05552.x.
11. **Stemberk V, Jones RP, Moroz O, Atkin KE, Edwards AM, Turkenburg JP, Leech AP, Massey RC, Potts JR**. 2014. Evidence for steric regulation of fibrinogen binding to *Staphylococcus aureus* fibronectin-binding protein A (FnBPA). J Biol Chem **289:**12842–12851. http://dx.doi.org/10.1074/jbc.M113.543546.
12. **Bustanji Y, Arciola CR, Conti M, Mandello E, Montanaro L, Samorí B**. 2003. Dynamics of the interaction between a fibronectin molecule and a living bacterium under mechanical force. Proc Natl Acad Sci U S A **100:**13292–13297. http://dx.doi.org/10.1073/pnas.1735343100.
13. **Xu CP, Boks NP, de Vries J, Kaper HJ, Norde W, Busscher HJ, van der Mei HC**. 2008. *Staphylococcus aureus*-fibronectin interactions with and without fibronectin-binding proteins and their role in adhesion and desorption. Appl Environ Microbiol **74:**7522–7528. http://dx.doi.org/10.1128/AEM.00948-08.
14. **Buck AW, Fowler VG, Jr, Yongsunthon R, Liu J, DiBartola AC, Que YA, Moreillon P, Lower SK**. 2010. Bonds between fibronectin and fibronectin-binding proteins on *Staphylococcus aureus* and *Lactococcus lactis*. Langmuir **26:**10764–10770. http://dx.doi.org/10.1021/la100549u.
15. **Lower SK, Yongsunthon R, Casillas-Ituarte NN, Taylor ES, DiBartola AC, Lower BH, Beveridge TJ, Buck AW, Fowler VG, Jr.** 2010. A tactile response in *Staphylococcus aureus*. Biophys J **99:**2803–2811. http://dx.doi.org/10.1016/j.bpj.2010.08.063.
16. **Casillas-Ituarte NN, Lower BH, Lamlertthon S, Fowler VG, Jr, Lower SK**. 2012. Dissociation rate constants of human fibronectin binding to fibronectin-binding proteins on living *Staphylococcus aureus* isolated from clinical patients. J Biol Chem **287:**6693–6701. http://dx.doi.org/10.1074/jbc.M111.285692.
17. **Emerson RJ, Bergstrom TS, Liu Y, Soto ER, Brown CA, McGimpsey WG, Camesano TA**. 2006. Microscale correlation between surface chemistry, texture, and the adhesive strength of *Staphylococcus epidermidis*. Langmuir **22:**11311–11321. http://dx.doi.org/10.1021/la061984u.
18. **Peters BM, Ovchinnikova ES, Krom BP, Schlecht LM, Zhou H, Hoyer LL, Busscher HJ, van der Mei HC, Jabra-Rizk MA, Shirtliff ME**. 2012. *Staphylococcus aureus* adherence to *Candida albicans* hyphae is mediated by the hyphal adhesin ALS:3p. Microbiology **158:**2975–2986. http://dx.doi.org/10.1099/mic.0.062109-0.
19. **Zeng G, Müller T, Meyer RL**. 2014. Single-cell force spectroscopy of bacteria enabled by naturally derived proteins. Langmuir **30:**4019–4025. http://dx.doi.org/10.1021/la404673q.
20. **Alsteens D, Beaussart A, El-Kirat-Chatel S, Sullan RM, Dufrêne YF**. 2013. Atomic force microscopy: a new look at pathogens. PLoS Pathog **9:**e1003516. http://dx.doi.org/10.1371/journal.ppat.1003516.
21. **Dufrêne YF**. 2014. Atomic force microscopy in microbiology: new structural and functional insights into the microbial cell surface. mBio **5**(4): e01363-14. http://dx.doi.org/10.1128/mBio.01363-14.
22. **Beaussart A, El-Kirat-Chatel S, Herman P, Alsteens D, Mahillon J, Hols P, Dufrêne YF**. 2013. Single-cell force spectroscopy of probiotic bacteria. Biophys J **104:**1886–1892. http://dx.doi.org/10.1016/j.bpj.2013.03.046.
23. **Beaussart A, El-Kirat-Chatel S, Sullan RM, Alsteens D, Herman P, Derclaye S, Dufrêne YF**. 2014. Quantifying the forces guiding microbial cell adhesion using single-cell force spectroscopy. Nat Protoc **9:**1049–1055. http://dx.doi.org/10.1038/nprot.2014.066.
24. **El-Kirat-Chatel S, Mil-Homens D, Beaussart A, Fialho AM, Dufrêne YF**. 2013. Single-molecule atomic force microscopy unravels the binding mechanism of a *Burkholderia cenocepacia* trimeric autotransporter adhesin. Mol Microbiol **89:**649–659. http://dx.doi.org/10.1111/mmi.12301.
25. **Fritz J, Katopodis AG, Kolbinger F, Anselmetti D**. 1998. Force-mediated kinetics of single p-selectin/ligand complexes observed by atomic force microscopy. Proc Natl Acad Sci U S A **95:**12283–12288. http://dx.doi.org/10.1073/pnas.95.21.12283.
26. **King NP, Beatson SA, Totsika M, Ulett GC, Alm RA, Manning PA, Schembri MA**. 2011. UafB is a serine-rich repeat adhesin of *Staphylococcus saprophyticus* that mediates binding to fibronectin, fibrinogen and human uroepithelial cells. Microbiology **157:**1161–1175. http://dx.doi.org/10.1099/mic.0.047639-0.
27. **King NP, Sakinç T, Ben Zakour NL, Totsika M, Heras B, Simerska P, Shepherd M, Gatermann SG, Beatson SA, Schembri MA**. 2012. Characterisation of a cell wall-anchored protein of *Staphylococcus saprophyticus* associated with linoleic acid resistance. BMC Microbiol **12:**8. http://dx.doi.org/10.1186/1471-2180-12-8.
28. **Xu LC, Siedlecki CA**. 2012. Effects of plasma proteins on *Staphylococcus epidermidis* RP62A adhesion and interaction with platelets on polyurethane biomaterial surfaces. J Biomater Biotechnol **3:**487–498. http://dx.doi.org/10.4236/jbnb.2012.324050.
29. **Oesterhelt F, Oesterhelt D, Pfeiffer M, Engel A, Gaub HE, Müller DJ**. 2000. Unfolding pathways of individual bacteriorhodopsins. Science **288:**143–146. http://dx.doi.org/10.1126/science.288.5463.143.
30. **Herman P, El-Kirat-Chatel S, Beaussart A, Geoghegan JA, Foster TJ, Dufrêne YF**. 2014. The binding force of the staphylococcal adhesin SdrG is remarkably strong. Mol Microbiol **93:**356–368. http://dx.doi.org/10.1111/mmi.12663.
31. **Alsteens D, Van Dijck P, Lipke PN, Dufrêne YF**. 2013. Quantifying the forces driving cell-cell adhesion in a fungal pathogen. Langmuir **29:**13473–13480. http://dx.doi.org/10.1021/la403237f.
32. **Francius G, Domenech O, Mingeot-Leclercq MP, Dufrêne YF**. 2008. Direct observation of *Staphylococcus aureus* cell wall digestion by lysostaphin. J Bacteriol **190:**7904–7909. http://dx.doi.org/10.1128/JB.01116-08.
33. **Baumgartner W, Hinterdorfer P, Ness W, Raab A, Vestweber D, Schindler H, Drenckhahn D**. 2000. Cadherin interaction probed by atomic force microscopy. Proc Natl Acad Sci U S A **97:**4005–4010. http://dx.doi.org/10.1073/pnas.070052697.
34. **Verbelen C, Raze D, Dewitte F, Locht C, Dufrêne YF**. 2007. Single-molecule force spectroscopy of mycobacterial adhesin-adhesin interactions. J Bacteriol **189:**8801–8806. http://dx.doi.org/10.1128/JB.01299-07.
35. **Hinterdorfer P, Baumgartner W, Gruber HJ, Schilcher K, Schindler H**. 1996. Detection and localization of individual antibody-antigen recognition events by atomic force microscopy. Proc Natl Acad Sci U S A **93:**3477–3481. http://dx.doi.org/10.1073/pnas.93.8.3477.
36. **Vergara-Irigaray M, Valle J, Merino N, Latasa C, García B, Ruiz de los Mozos I, Solano C, Toledo-Arana A, Penadés JR, Lasa I**. 2009. Relevant role of fibronectin-binding proteins in *Staphylococcus aureus* biofilm-associated foreign-body infections. Infect Immun **77:**3978–3991. http://dx.doi.org/10.1128/IAI.00616-09.
37. **Barbu EM, Mackenzie C, Foster TJ, Höök M**. 2014. SdrC induces staphylococcal biofilm formation through a homophilic interaction. Mol Microbiol **94:**172–185. http://dx.doi.org/10.1111/mmi.12750.
38. **Otto M**. 2014. Physical stress and bacterial colonization. FEMS Microbiol Rev **38:**1250–1270. http://dx.doi.org/10.1111/1574-6976.12088.
39. **Geoghegan JA, Corrigan RM, Gruszka DT, Speziale P, O'Gara JP, Potts JR, Foster TJ**. 2010. Role of surface protein SasG in biofilm formation by *Staphylococcus aureus*. J Bacteriol **192:**5663–5673. http://dx.doi.org/10.1128/JB.00628-10.
40. **Conrady DG, Brescia CC, Horii K, Weiss AA, Hassett DJ, Herr AB**. 2008. A zinc-dependent adhesion module is responsible for intercellular

adhesion in staphylococcal biofilms. Proc Natl Acad Sci U S A **105:** 19456–19461. http://dx.doi.org/10.1073/pnas.0807717105.

41. **Conrady DG, Wilson JJ, Herr AB**. 2013. Structural basis for Zn^{2+}-dependent intercellular adhesion in staphylococcal biofilms. Proc Natl Acad Sci U S A **110:**E202–E211. http://dx.doi.org/10.1073/pnas.1208134110.
42. **Becker KW, Skaar EP**. 2014. Metal limitation and toxicity at the interface between host and pathogen. FEMS Microbiol Rev **38:**1235–1249. http://dx.doi.org/10.1111/1574-6976.12087.
43. **Kehl-Fie TE, Skaar EP**. 2010. Nutritional immunity beyond iron: a role for manganese and zinc. Curr Opin Chem Biol **14:**218–224. http://dx.doi.org/10.1016/j.cbpa.2009.11.008.
44. **Zalewski P, Truong-Tran A, Lincoln S, Ward D, Shankar A, Coyle P, Jayaram L, Copley A, Grosser D, Murgia C, Lang C, Ruffin R**. 2006. Use of a zinc fluorophore to measure labile pools of zinc in body fluids and cell-conditioned media. Biotechniques **40:**509–520. http://dx.doi.org/10.2144/06404RR02.
45. **Rice KC, Mann EE, Endres JL, Weiss EC, Cassat JE, Smeltzer MS, Bayles KW**. 2007. The cidA murein hydrolase regulator contributes to DNA release and biofilm development in *Staphylococcus aureus*. Proc Natl Acad Sci U S A **104:**8113–8118. http://dx.doi.org/10.1073/pnas.0610226104.
46. **Katayama A, Tsujii A, Wada A, Nishino T, Ishihama A**. 2002. Systematic search for zinc-binding proteins in *Escherichia coli*. FEBS J **269:**2403–2413. http://dx.doi.org/10.1046/j.1432-1033.2002.02900.x.
47. **Cassat JE, Hammer ND, Campbell JP, Benson MA, Perrien DS, Mrak LN, Smeltzer MS, Torres VJ, Skaar EP**. 2013. A secreted bacterial protease tailors the *Staphylococcus aureus* virulence repertoire to modulate bone remodeling during osteomyelitis. Cell Host Microbe **13:**759–772. http://dx.doi.org/10.1016/j.chom.2013.05.003.
48. **Berquand A, Xia N, Castner DG, Clare BH, Abbott NL, Dupres V, Adriaensen Y, Dufrêne YF**. 2005. Antigen binding forces of single antilysozyme Fv fragments explored by atomic force microscopy. Langmuir **21:**5517–5523. http://dx.doi.org/10.1021/la050162e.